JOURNAL OF APPLIED ELECTROCHEMISTRY 20 (1990) 69–76

Electrochemical dissolution of stainless steels in flow channel cells with and without photoresist masks

E. ROSSET, M. DATTA*, D. LANDOLT

Swiss Federal Institute of Technology, Materials Department, CH-1007 Lausanne, Switzerland

Received 1 September 1988

High rate anodic dissolution of Fe, Fe13Cr, Fe24Cr, Cr and AISI type 304 stainless steel is studied in NaCl and $NaNO_3$ using a flow channel cell with well-defined hydrodynamic conditions. The apparent valence for dissolution and the surface finish are investigated as a function of current density. Electrochemical etching experiments through photoresist masks are performed with type 304 stainless steel using $NaNO_3$. The influence of current density on the shape and surface finish of the etch grooves and the uniformity of the attack between differently spaced grooves can be qualitatively explained from the electrochemical data obtained on flat electrodes.

1. Introduction

Electrochemical machining (ECM) is a metal-shaping process involving anodic dissolution at high rate with small interelectrode gaps [1]. The rational evaluation of optimum reaction conditions and the theoretical modeling of the process require knowledge of the stoichiometry and of the rate limiting step of the dissolution process. Electrochemical micromachining through photoresist masks (EMM) is a new electrochemical machining process which can be used to shape thin foil materials using photolithographic techniques as in chemical milling [2–6]. Most studies of EMM deal with chemically resistant materials like tantalum or molybdenum and aggressive electrolytes including strong acids or bases [3–5]. During the course of the present study a paper by Chatterjee appeared describing EMM of small holes in a variety of sheet materials including stainless steel plate using neutral $NaNO_3$ and NaCl electrolytes [6]. The literature on EMM is mostly of a technological nature and very little information on the role of prevailing electrochemical conditions is available.

The purpose of the present study is to provide information on the high rate dissolution behavior of stainless steels in NaCl and $NaNO_3$ electrolytes and to identify critical factors which affect EMM of these materials by performing dissolution experiments through photoresist masks.

The kinetics and stoichiometry of high rate anodic dissolution of stainless steels in neutral electrolytes are not well known but the anodic behavior of Fe and Ni has been studied by a number of authors [7–14]. For iron dissolution in chloride solutions the stoichiometry and the resulting surface finish depend strongly on mass transport conditions at the electrode [7, 8]. Below the limiting current corresponding to salt film precipitation dissolution yields Fe^{2+} ions while above the limiting current Fe^{2+} and Fe^{3+} ions are produced simultaneously and surface brightening is observed [7]. In nitrate electrolytes high rate iron dissolution takes place in the transpassive potential region only and is accompanied by oxygen evolution. Metal dissolution efficiency increases with increasing current density and is strongly influenced by local temperature changes [8].

Active dissolution of chromium in acid solutions leads to production of Cr^{2+} [15, 16], while in the passive potential region, chromium dissolves as Cr^{3+} [9]. In neutral ECM electrolytes anodic dissolution of chromium takes place in the transpassive potential region yielding Cr^{6+} independent of current density and of the nature of the electrolyte anions [10, 14]. However, it has been reported that dissolution of Ni–Cr alloys with a Cr content of less than 20% in chloride solutions leads to Cr^{3+} the potential being lower than that necessary for transpassive dissolution of pure Cr [11].

2. Experimental details

2.1. *High rate dissolution under controlled mass transport conditions*

The high rate dissolution behavior of Fe, Cr, Fe13Cr, Fe24Cr and AISI type 304 stainless steel (SS304) was investigated in a channel flow cell allowing for well-defined mass transport conditions. The flow cell and experimental apparatus are described elsewhere in detail [7]. The anodes, 1 cm long and 0.3 cm wide, were positioned flush with the wall of a 0.3 cm wide channel at a distance of 0.05 cm from a nickel cathode having the same dimensions as the anode. Unless otherwise stated, a constant electrolyte flow velocity of 2.5 m s^{-1} was employed and the temperature was maintained constant at 25° C.

* *Present address*: IBM Corp., T. J. Watson Research Center, Yorktown Heights, NY 10598, USA.

0021-891X/90 $03.00 + .12

Table 1. Composition of different metals and alloys employed in the present investigation

Material	*Mn*	*Si*	*S*	*P*	*C*	*O*	*Ni*	*Cr*	*Fe*
Fe	0.035	0.002	0.025	0.015	0.02	–	–	–	rest
Fe-13 Cr	< 0.001	0.033	0.004	0.005	0.032	0.0407	0.004	12.83	rest
Fe-24 Cr	0.002	0.043	0.006	0.004	0.033	0.1099	0.006	24.3	rest
304 stainless steel	1.50	0.61	0.030	0.040	0.06	–	10.1	18.0	rest
Cr	< 0.0001	< 0.001	–	–	–	0.210	–	rest	–

(–) indicates not determined.

The composition of metals and alloys investigated is given in Table 1. The anodes were mechanically polished on 600 emery paper, cleaned and cathodically pretreated in 0.1 M NaOH at 30 mA cm^{-2} for 5 min.

One series of experiments was aimed at comparing the anodic polarization behavior of different materials investigated. For that purpose, potentiodynamic current voltage curves were determined at a scan rate of 50 mV s^{-1}. Anode potentials, reported against the normal hydrogen electrode (NHE), were measured against a saturated calomel electrode (SCE) or a mercury sulphate electrode (MSE) connected to the channel by a backside capillary. A second series of experiments was aimed at the study of dissolution stoichiometry and of surface finish. For this the anode was dissolved galvanostatically by applying a constant charge of 60 C cm^{-2}. Anodes were weighed before and after dissolution to determine the weight loss. Surfaces resulting from dissoluton were examined by optical or scanning electron microscopy.

2.2. *Etching through photoresist masks*

Patterned anodes as shown in Fig. 1 were used. A series of 6 parallel rectangular electrodes 500 μm wide and 1 or 2 cm long were arranged in such a way that the distance between them was w, $2w$, $4w$, etc. where $w = 500\,\mu$m is the electrode width. The pattern also contained a 90° angle but its etching behavior was not studied here. The anode pattern covered an area of 2 cm × 2 cm. It was produced by photolithography on a 5 cm × 5 cm sheet of SS304 or 500 μm thickness. The photoresist resin (negative type, Riston, Du Pont) in the form of a 20 μm sheet was applied by cold-rolling to the stainless steel plate pretreated with a flash of nickel to improve adhesion.

The anode plate was placed in a channel flow cell opposite a cathode of stainless steel. The channel cell was 2 cm wide and 1 cm high, its total length being 7 cm. The electrodes were placed flush with the wall. The hydrodynamic conditions in this cell were less well defined than in the dissolution experiments on flat electrodes since it did not contain a hydrodynamic entrance length sufficiently long to establish a fully developed velocity profile. This is not a major problem however, because the hydrodynamic conditions with the forming etch grooves are mainly determined by the geometry of the groove. The electrolyte was circulated through the cell by means of a centrifugal pump. The flow rate was measured with rotameters and controlled with a regulating valve. A thermostated electrolyte tank was employed to maintain the temperature at 25° C. The flow rate corresponded to a Reynolds number of 1000. The anodes were positioned perpendicular to the flow direction. Etching experiments were carried out at constant current densities of 0.5, 3 and 15 A cm^{-2}. After passage of a predetermined amount of charge, typically 20, 100, 300 or 600 C, the patterned anode was removed from the cell and the shape of the etch profiles and/or their surface roughness was studied.

To study the shape changes resulting from dissolution the anode plate was cast into a polymeric resin and 5 parallel cuts at different positions were made perpendicular to the surface. The profile shape was photographed using a microscope. From the photograph the profile was digitized. From the

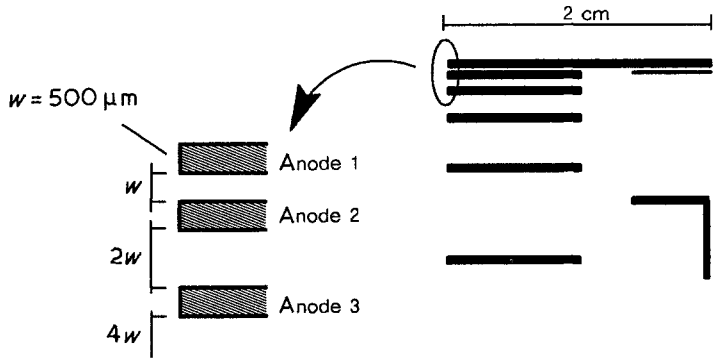

Fig. 1. Anode pattern used for EMM through photoresist masks.

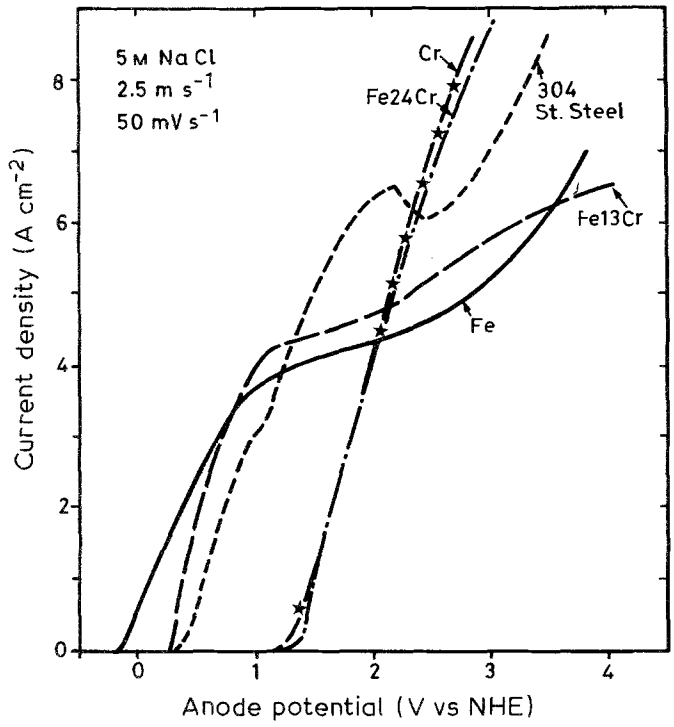

Fig. 2. Potentiodynamic polarization curves in 5 M NaCl.

digitized profiles different shape parameters could be derived and plots could be produced using a HP 9845 desk top computer [17]. For the purpose of the present study only the cross sectional area was evaluated.

3. Results

3.1. *High rate dissolution in channel flow cell*

A first series of experiments was carried out in 5 M NaCl. Figure 2 shows potentiodynamic current voltage curves measured at a scan rate of 50 mV s^{-1}. Both Fe and Fe13Cr exhibit a current plateau due to formation of a salt film consisting of $FeCl_2$ [12]. The plateau current is mass transport controlled and, therefore, varies with flow rate [7, 12]. Within the current density range studied, Fe24Cr and Cr which dissolve in the transpassive potential region do not exhibit a plateau. The anodic behavior of SS304 resembles that of Fe13Cr but the plateau is reached at a higher current density and presents a maximum. The nature of the surface film formed was not investigated but, by analogy to the behavior of Fe, Fe13Cr and of pure Ni [7], it is thought to consist of a mixed iron–nickel chloride.

The apparent valence of dissolution, n, was determined from the weight loss measured in galvanostatic experiments using Equation 1

$$n = \frac{MIt}{\Delta WF} \tag{1}$$

Here M is the atomic weight, I is the current, t is the dissolution time, ΔW is the weight loss and F is the Faraday constant. The atomic weight of the alloys was calculated by Equation 2

$$M_{\text{alloy}} = \Sigma x_j M_j \tag{2}$$

with x_j is the mole fraction of component j and M_j its atomic weight.

Results obtained at different current densities are presented in Fig. 3. For Fe and Fe13Cr below the limiting current $n = 2.0$ and $n = 2.1$, respectively; above the limiting current $n = 2.5$ and $n = 2.7$, respectively. The values for iron are consistent with previous data [7]; Fe^{2+} forms below the limiting current, whereas both Fe^{2+} and Fe^{3+} form above the limiting current. The measured values for Fe13Cr can be explained by postulating formation of Fe^{2+} and Cr^{2+} or Cr^{3+} below the limiting current and formation of Fe^{2+}, Fe^{3+} and Cr^{6+} (chromate) above the limting current. Pure Cr yielded $5 < n < 6$ indicting mostly chromate formation. The deviation from the theoretical value of $n = 6$ could, in part, be due to the presence of oxide inclusions in the chromium employed. The Fe24Cr yields $n = 3.6$ independent of current density. The theoretical value corresponding to formation of Fe^{3+} and Cr^{6+} is $n = 3.76$, in reasonable agreement with the measurement. For SS304 the experimental data yield $n = 3.5$ independent of current density. This corresponds to formation of Fe^{3+}, Cr^{6+} and Ni^{2+}.

Figure 4 presents mircographs which illustrate the surface morphology resulting from dissolution of the three alloys. The SEM micrographs a–c show surfaces after dissolution at 1 A cm^{-2} for Fe13Cr, Fe24Cr and SS304, respectively. The first two alloys exhibit surface etching, the latter pitting. At 20 A cm^{-2} the surface finish resulting from dissolution was similar for all three alloys and corresponded to that shown in the optical micrograph (d).

Anodic dissolution in $NaNO_3$ takes place in the transpassive potential region. This is illustrated by the potentiodynamic polarization curves of Fig. 5. The

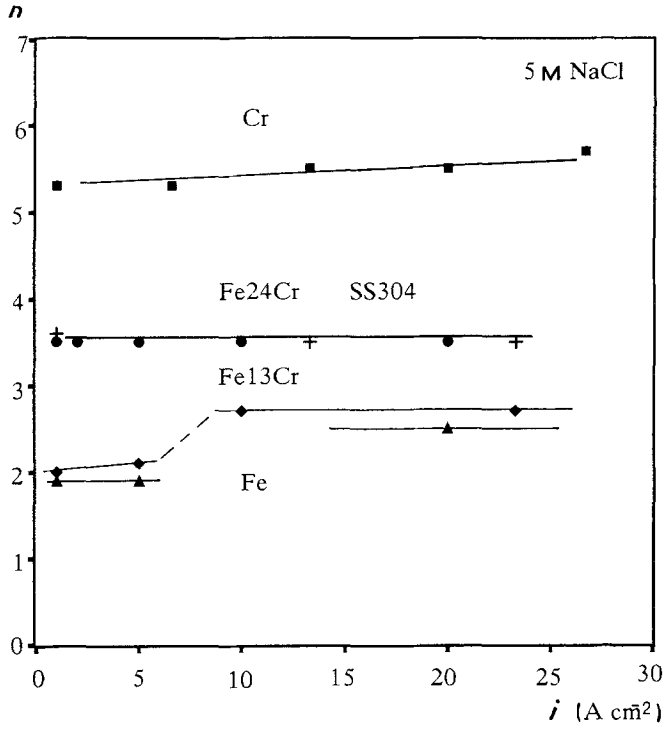

Fig. 3. Apparent valence of dissolution in 5 M NaCl derived from galvanostatic experiments at 2.5 m s^{-1}.

transpassive potential region for Cr starts at 1.36 V (NHE), for iron and for the alloys at 1.76 V. The apparent valence of dissolution for Fe, Cr and SS304 is shown in Fig. 6. In 6 M $NaNO_3$ chromium dissolves to the hexavalent state at all current densities. At current densities < 5 A cm^{-2} the value of n for iron becomes very high, because the predominant reaction is oxygen evolution. The minimum observed at 15 A cm^{-2} may be due to the fact that the current efficiency for iron dissolution in nitrate electrolytes

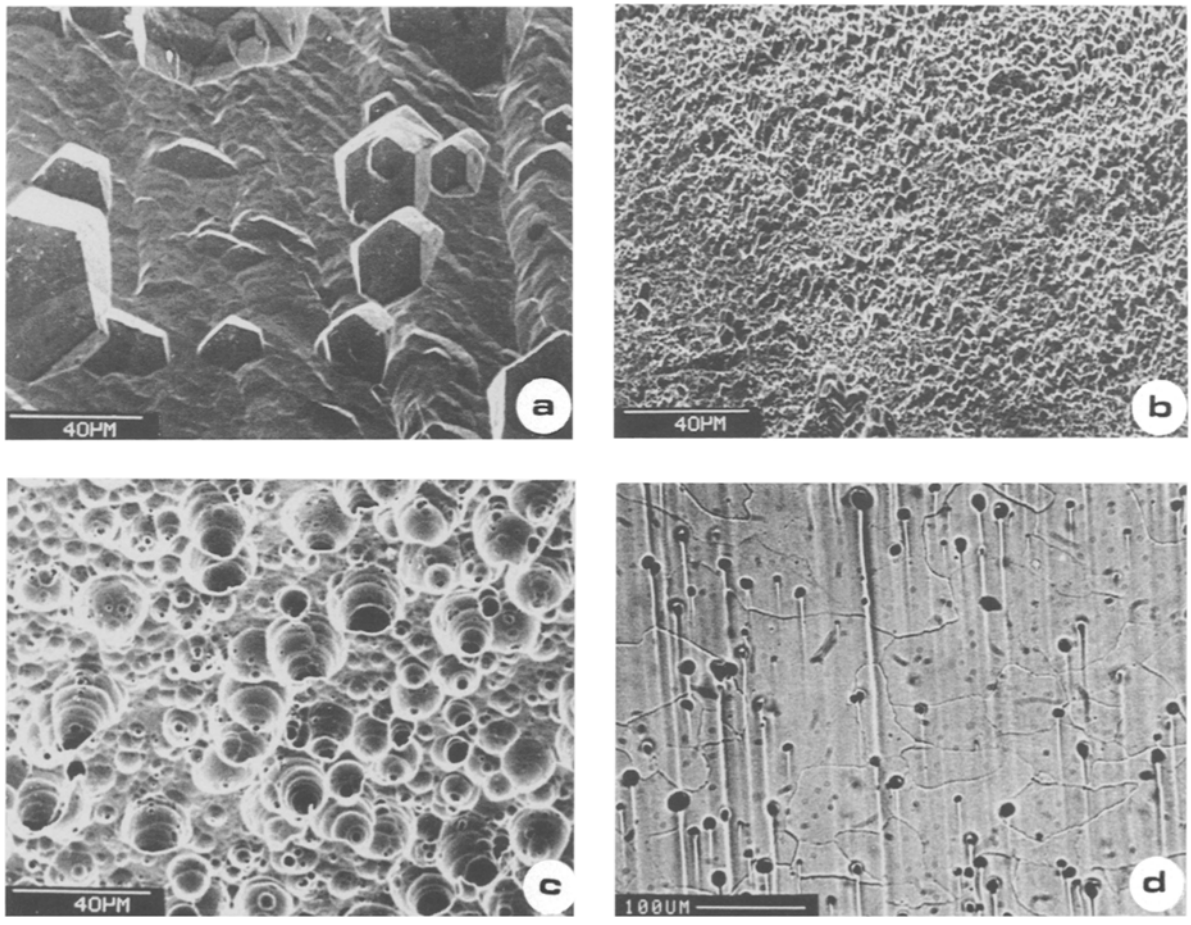

Fig. 4. Micrographs of surfaces after dissolution in 5 M NaCl at 2.5 m s^{-1}. (a) Fe13Cr, 1 A cm^{-2}; (b) Fe24Cr, 1 A cm^{-2}; (c) SS304, 1 A cm^{-2}; (d) SS304, 20 A cm^{-2}.

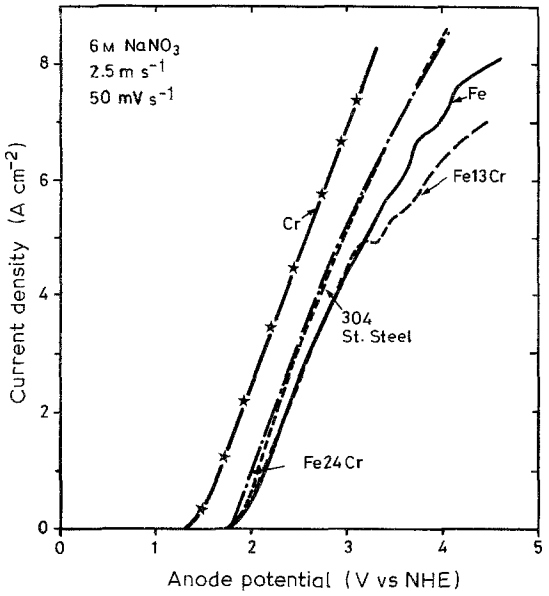

Fig. 5. Potentiodynamic polarization curves in 6 M $NaNO_3$.

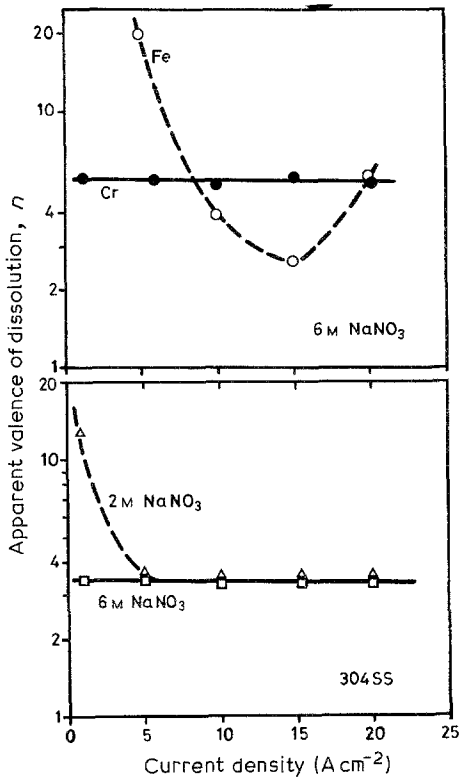

Fig. 6. Apparent valence of dissolution in $NaNO_3$ derived from galvanostatic experiments at 2.5 m s^{-1}.

depends strongly on the local temperature [8] and heating effects cannot be excluded under the present conditions at high current densities. The apparent valence of dissolution of SS304 in 6 M $NaNO_3$ is $n = 3.4$ independent of current density. It corresponds to formation of Fe^{3+}, Ni^{2+} and Cr^{6+} (the theoretical value is $n = 3.48$). In 2 M $NaNO_3$ oxygen evolution at current densities below 5 A cm^{-2} leads to a higher n.

The polarization data of Fig. 5 do not show a limiting current region. However, the analysis of galvanostatic transients measured with SS304 indicates that anodic salt film formation occurs above a critical current density. Figure 7 shows such transients measured at a flow velocity of 2.5 m s^{-1} in 6 M $NaNO_3$ at different current densities. Transients above 10 A cm^{-2} exhibit the characteristic overshoots associated with salt film formation [7]. In Fig. 8 scanning electron micrographs of surfaces after dissolution are shown. At 1 A cm^{-2} the surface is rough. The morphology suggests that a pitting-type breakdown of the passive film occurred because some parts of the original surface are still intact. At 28 A cm^{-2} the entire surface is smooth and bright. The observed behaviour is similar to that previously found for transpassive dissolution of Nickel in $NaNO_3$ where the transition from surface roughening to brightening was found to coincide with salt film precipitation and, therefore, was mass transport controlled [18]. Experiments performed in the present study at two different flow rates confirmed that the transition occurred at lower cur-

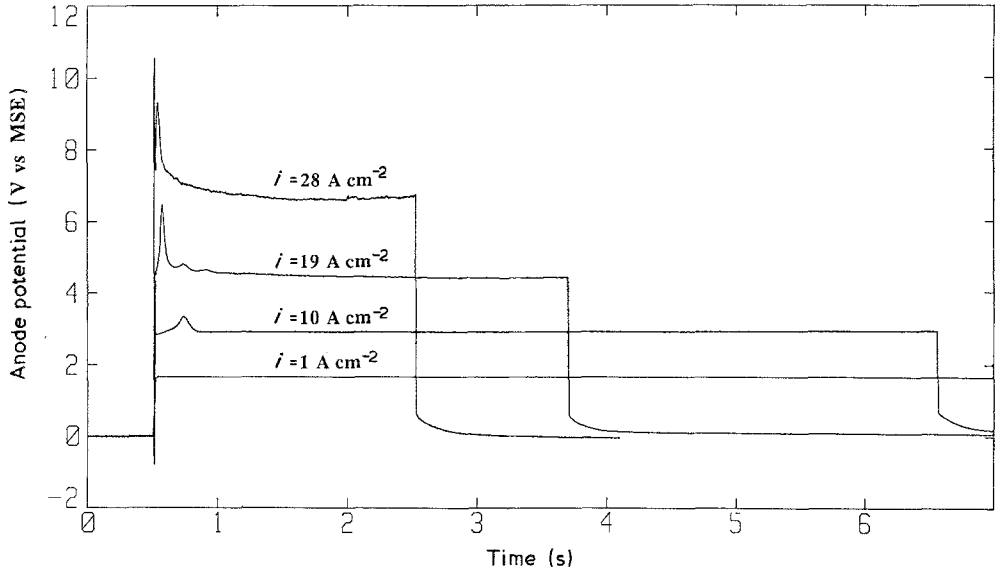

Fig. 7. Potential transients measured upon application of a current pulse to a SS304 anode in 6 M $NaNO_3$. Flow rate: 2.5 m s^{-1}.

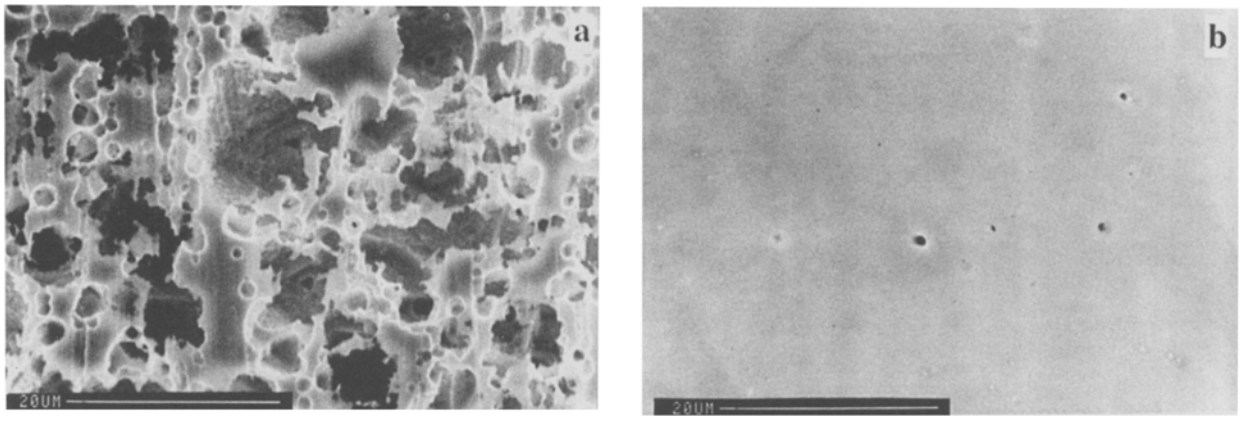

Fig. 8. Surface texture of SS304 resulting from dissolution in 6 M $NaNO_3$ at 1 A cm^{-2} (a) and 28 A cm^{-2} (b). Flow rate: 2.5 m s^{-1}. Applied charge: 60 C cm^{-2}.

rent density when the flow rate was decreased to 1 m s^{-1} lending support to the hypothesis that the same mechanism governs surface brightening of SS304. A quantitative evaluation of the transport processes was not made, however.

3.2. *Etching through photoresist masks*

From the above experiments it follows that both NaCl and $NaNO_3$ can be used for EMM. Because of its passivating character $NaNO_3$ is less corrosive to equipment and, therefore, only this electrolyte was used for further studies. Figure 9 shows profile shapes resulting from dissolution at 0.5, 3 and 15 A cm^{-2} (based on the initial anode area) in 6 M $NaNO_3$ at a Reynolds number of Re = 1000. The total charge applied in the different experiments is also indicated. A current density of 0.5 A cm^{-2} led to extreme roughening and ill-defined profile shape. At 3 A cm^{-2} smooth surfaces were produced and the profile shape exhibited a slight asymetry. At 15 A cm^{-2} electrolyte heating in the etch groove led to a deterioration of the precision of the attack and to poor reproducibility.

From the measured cross-section of a given anode an equivalent volume of dissolved metal was calculated by multiplying with the total length and from this an apparent charge was computed using the Faraday law with n = 3.4. The results are shown in Fig. 10. They indicate that at 0.5 A cm^{-2} the current distribution between anodes was highly non-uniform, dissolution of anode No. 6 being almost twice as rapid as that of anodes No. 1–3. The non-uniformity in the rate of attack is caused by differences in anode spacing. The latter increased with increasing anode number (Fig.1). At 3 A cm^{-2} the attack was more uniform. The reasons for this will be discussed below. At 15 A cm^{-2} a discontinuity was observed between anodes No. 2 and 3. The behaviour is due to the thermal effects mentioned above.

4. Discussion

The present data confirm the feasibility of using $NaNO_3$ and NaCl for EMM of stainless steels but they also point out inherent problems of the process. The value of applied current density and the convection

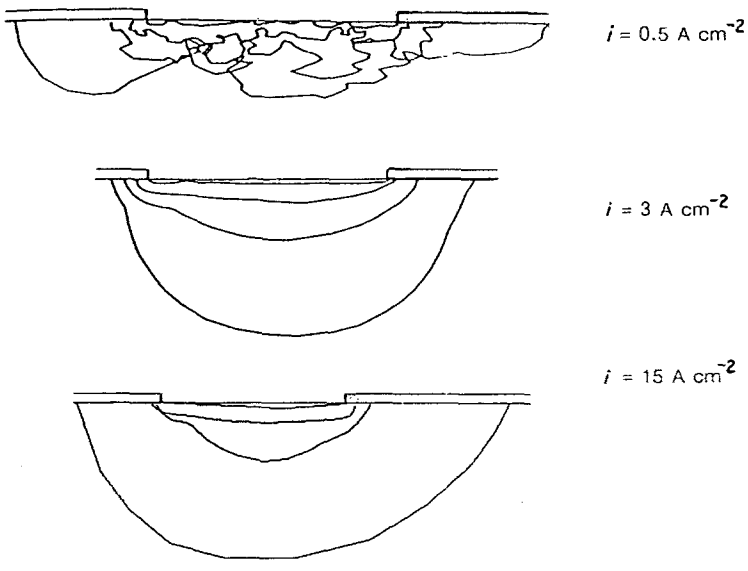

Fig. 9. Profile shapes of anode No. 3 corresponding to different charges of 20, 100, 300 and 600 C. Current density: 0.5 A cm^{-2}, 3 A cm^{-2}, 15 A cm^{-2}. Reynolds number 1000.

conditions strongly influence the shape of the etch profiles, the surface roughness and the uniformity of the attack among differently spaced anodes. The electrochemical data obtained in the flow channel cell allow comment on some of these factors.

Two dissolution modes are distinguished in Fig. 7 depending on applied current density. They will be referred to as 'below the limiting current' and 'above the limiting current' in analogy with previous observations with nickel [18]. The EMM results of Fig. 9 agree qualitatively with the data of Fig. 8. At $0.5\,A\,cm^{-2}$ a very rough surface results from dissolution, while at $3\,A\,cm^{-2}$ brightening occurs indicating that dissolution takes place above the limiting current. On flat electrodes with fully developed channel flow at $2.6\,m\,s^{-1}$ the transition between the two dissolution modes occurs at $8–10\,A\,cm^{-2}$. The hydrodynamic conditions in a developing etch groove differ from those on flat electrodes and the prevailing transport rates are expected to be lower. Therefore, it is reasonable that in the etching experiments with photoresist masks brightening is observed at $3\,A\,cm^{-2}$ already. It should be noted that the current density values indicated for the EMM experiments refer to the original (flat) area of the anode. The actual current density in a growing etch groove is, therefore, lower and the observed transition at $3\,A\,cm^{-2}$ indicates that low mass transport rates prevailed in the etch groove.

The dissolution mode affects the current distribution between the anodes in EMM. According to Fig. 10 the different anodes are attacked more uniformly at $3\,A\,cm^{-2}$ than at $0.5\,A\,cm^{-2}$. Below the limiting current the distribution between the anodes is given by the electrical field in the interelectrode gap. This explains that at $0.5\,A\,cm^{-2}$ widely spaced anodes dissolve faster [17]. The more uniform attack at $3\,A\,cm^{-2}$ can be explained in two possible ways. On the one hand, if dissolution occurs at the limiting current, it is controlled by the rate of transport of dissolution products from the anode into the bulk. The non-uniformity of the electrical field, therefore, plays a minor role, the rate of attack being governed by local hydrodynamic conditions. On the other hand, even if dissolution is not controlled by mass transport the accumulation of solid dissolution products in the etch groove increases the local ohmic resistance which, relatively to the overall cell resistance, becomes more important. As a consequence, the current density at different anodes becomes more uniform. Both of these effects may have played a role in the present experiments but the mass transport theory is supported by the profile shape at $3\,A\,cm^{-2}$ (Fig. 9) which exhibits a marked asymmetry in the fluid flow direction. Indeed, calculations by Alkire and Reiser [19] suggest that the hydrodynamic conditions in an etch groove under laminar channel flow conditions lead to a higher mass transport rate on the downstream part of the groove. For mass transport-controlled etching this should result in an asymmetric profile shape qualitatively similar to that observed in Fig. 9 at $3\,A\,cm^{-2}$. Very recently, Alkire and Deligianni showed that the asymmetry depends on the aspect ratio of the etch profile because the latter affects the hydrodynamic conditions in the etch groove [20].

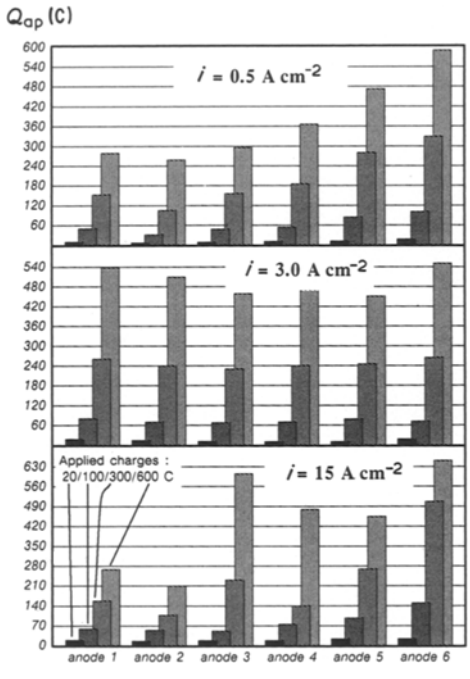

Fig. 10. Apparent charge calculated for anodes 1–6 from the measured profile shapes at 0.5, 3.0 and $15\,A\,cm^{-2}$ and at applied charges of 20, 10, 300 and 600 C. Reynolds number: 1000.

5. Conclusion

(1) Stainless steel 304 in 6 M $NaNO_3$ dissolves electrochemically in the transpassive mode with an apparent valence of dissolution of $n = 3.4$. The surface finish resulting from dissolution is governed by prevailing mass transport conditions.

(2) In electrochemical micromachining through photoresist masks in a flow channel the current distribution between anodes and hence the etch depth is more uniform if dissolution takes place under mass transport control but the resulting profiles may exhibit an asymmetry in flow direction.

(3) The maximum current density that can be applied in electrochemical micromachining is limited by Joule heating of the electrolyte in the developing etch grooves.

Acknowledgements

The present study was financially supported by CERS, Berne. CMT Rickenbach in La Chaux-de-Fonds fabricated the patterned electrodes.

References

[1] J. A. McGeough, 'Principles of Electrochemical Machining', Chapman and Hall, London (1974) pp. 255.

[2] D. Landolt, 'Proc. Symp. Electrochemical Technology in the Electronics Industry', (edited by L. Rowankiw and T. Osaka), Electrochemical Soc., Princeton, New Jersey (1988) p. 573.

[3] D. M. Allen, 'The Principles and Practice of Photochemical Machining and Photoetching', Adam Hilger, Bristol and Boston (1986) pp. 190.
[4] W. C. Wicke, U.S. Patent 2,900,283 June 27 (1961).
[5] M. Hiermaier and H. Simon, *Galvanotechnik* **74** (1983) 401.
[6] B. Chatterjee, *Precision Eng.* **8** (1986) 131.
[7] M. Datta and D. Landolt, *Electrochim. Acta.* **25** (1980) 1255.
[8] M. Datta and D. Landolt, *Electrochim. Acta.* **25** (1980) 1263.
[9] Th. Heumann and H. S. Panesar, *J.E.C.S.* **110** (1963) 628.
[10] O. A. Arzhintar, A. I. Dikusar, V. I. Petrenko and Yu. N. Petrov, *Electron. Orab. Mater.* **6** (1974) 9.
[11] A. D. Davydov, E. N. Kiriyak and V. D. Kaschceev, *Elektrohimiya* **14** (1980) 1420.
[12] H. C. Kuo and D. Landolt, *Electrochim. Acta* **20** (1975) 393.
[13] D. T. Chin and K. W. Mao, *J. Appl. Electrochem.* **4** (1974) 155.
[14] D. Landolt, in 'Passivity of Metals' (edited by R. P. Frankenthal and J. Kruger), Electrochemical Soc. (1978) p. 484.
[15] M. S. El-Basionny and S. Haruyama, *Corros. Sci.* **17** (1977) 405.
[16] Gmelin, 'Handbook der anorganischen Chemie', Aufl. Nr. 52, Cr[A] (1968) p. 458.
[17] E. Rosset, Photodécoupage Electrochimique en Milieu Salin Neutre. Ph.D Thesis No. 731, EPFL, Lausanne (1988).
[18] M. Datta and D. Landolt, *J.E.C.S.* **122** (1975) 1466.
[19] R. C. Alkire and P. B. Reiser, *J.E.C.S.* **131** (1984) 2795.
[20] R. C. Alkire and H. Deligianni, *J.E.C.S.* **135** (1988) 1093.